Cancer Cell
Article

Loss of FBP1 by Snail-Mediated Repression Provides Metabolic Advantages in Basal-like Breast Cancer

Chenfang Dong,[1,5] Tingting Yuan,[1,5,11] Yadi Wu,[2,5,11] Yifan Wang,[1,5,11] Teresa W.M. Fan,[6] Sumitra Miriyala,[4,5] Yiwei Lin,[1,5] Jun Yao,[7] Jian Shi,[1,5] Tiebang Kang,[9] Pawel Lorkiewicz,[6] Daret St Clair,[4,5] Mien-Chie Hung,[8,10] B. Mark Evers,[1,3,5] and Binhua P. Zhou[1,5,*]

[1]Department of Molecular and Cellular Biochemistry
[2]Department of Molecular and Biomedical Pharmacology
[3]Department of Surgery
[4]Graduate Center for Toxicology
[5]Markey Cancer Center
The University of Kentucky, College of Medicine, Lexington, KY 40506, USA
[6]Center for Regulatory and Environmental Analytical Metabolomics, Department of Chemistry and J.G. Brown Cancer Center, University of Louisville, Louisville, KY 40202, USA
[7]Department of Neuro-Oncology
[8]Department of Molecular and Cellular Oncology
The University of Texas M. D. Anderson Cancer Center, Houston, TX 77030, USA
[9]State Key Laboratory of Oncology in South China, Guangzhou 510060, China
[10]Center for Molecular Medicine and Graduate Institute of Cancer Biology, China Medical University, Taichung, Taiwan
[11]These authors contributed equally to this study
*Correspondence: peter.zhou@uky.edu
http://dx.doi.org/10.1016/j.ccr.2013.01.022

SUMMARY

The epithelial-mesenchymal transition (EMT) enhances cancer invasiveness and confers tumor cells with cancer stem cell (CSC)-like characteristics. We show that the Snail-G9a-Dnmt1 complex, which is critical for E-cadherin promoter silencing, is also required for the promoter methylation of fructose-1,6-biphosphatase (FBP1) in basal-like breast cancer (BLBC). Loss of FBP1 induces glycolysis and results in increased glucose uptake, macromolecule biosynthesis, formation of tetrameric PKM2, and maintenance of ATP production under hypoxia. Loss of FBP1 also inhibits oxygen consumption and reactive oxygen species production by suppressing mitochondrial complex I activity; this metabolic reprogramming results in an increased CSC-like property and tumorigenicity by enhancing the interaction of β-catenin with T-cell factor. Our study indicates that the loss of FBP1 is a critical oncogenic event in EMT and BLBC.

INTRODUCTION

The increased motility and invasiveness of metastatic tumor cells are reminiscent of the events that occur at the epithelial-mesenchymal transition (EMT), a characteristic of embryonic development, tissue remodeling, and wound healing (Polyak and Weinberg, 2009; Thiery et al., 2009). EMT also bestows tumor cells with cancer stem cell (CSC)-like characteristics, providing them with therapeutic resistance and conferred tumor recurrence. Although metabolism plays a fundamental role in essentially every function of a cell, little is known about how the cell's metabolism contributes to the morphological and molecular changes in EMT. Understanding the causes and consequences of altered metabolism, particularly glucose, in EMT may permit the identification of drug targets for treating metastatic breast cancer.

Glucose homeostasis is reciprocally controlled by the catabolic glycolysis/oxidative phosphorylation (OXPHOS) and the

Significance

BLBC is associated with an aggressive clinical history, development of recurrence, distant metastasis, and shorter patient survival. BLBC contains abundant EMT markers and possesses many CSC-like characteristics, but the metabolic program associates with these changes remain unknown. We showed that the Snail-G9a-Dnmt1 complex repressed FBP1 expression in BLBC; this results in increased CSC-like characteristics and tumorigenicity by enhancing aerobic glycolysis and by suppressing ROS production. This metabolic reprogramming is intertwined with the development of BLBC, because loss of FBP1 is required for EMT induction, the conversion from luminal to basal-like phenotype, and is associated with poor patient survival. Our study suggests that targeting the Snail complex may be an effective approach for treating BLBC.

anabolic gluconeogenesis pathway. In the catabolic reaction, glucose is converted to pyruvate in the absence of oxygen, which can be further metabolized to lactate in the cytoplasm (glycolysis). In the presence of oxygen, pyruvate is channeled to the tricarboxylic acid (TCA) cycle to fuel OXPHOS for the maximal ATP production in the mitochondria. Otto Warburg noticed that some tumor cells preferentially metabolized glucose to lactate in the presence of ample oxygen, a process called aerobic glycolysis (Koppenol et al., 2011). Activation of several oncogenes contributes to the Warburg effect in tumor cells. For example, AKT1 stimulates glucose uptake by enhancing Glu-4 expression and by activating hexokinase (Elstrom et al., 2004; Robey and Hay, 2009). Activation of Myc also induces glycolysis by inducing LDH-A and PDK1 expression, which inhibits the conversion of pyruvate to acetyl-CoA and facilitates the production of lactate (Dang et al., 2008). Tumor cells can increase an embryonic form of pyruvate kinase M2 (PKM2) to trigger glycolysis in lung cancer (Christofk et al., 2008).

Much attention has focused on regulation of the catabolic pathway of glucose. Gluconeogenesis is less investigated and may play an equally important role in the switch to aerobic glycolysis in tumor cells. Fructose-1,6-bisphosphatase (FBP1), which catalyzes the splitting of fructose-1,6-bisphosphate (F-1,6-BP) into fructose 6-phosphate and inorganic phosphate, is a rate-limiting enzyme in gluconeogenesis. An autosomal recessive inherited disorder of FBP1 deficiency is characterized by hypoglycemia and lactic acidosis, which often causes sudden infant death (Emery et al., 1988). This suggests that loss of FBP1 increases glucose uptake and glycolysis, leading to hypoglycemia and lactic acidosis in patients. Consistent with these observations, inhibition of FBP1 significantly increases glucose sensitivity and utilization in type 2 diabetic mouse models (van Poelje et al., 2006). Interestingly, loss of FBP1 expression due to promoter DNA methylation has been observed in liver, colon, and gastric cancers (Chen et al., 2011; Liu et al., 2010), suggesting that epigenetic regulation of FBP1 plays a critical role in modulating glucose metabolism in cancer.

Breast cancer can be divided into four subtypes based on gene expression profiling: luminal A, luminal B, HER2, and basal-like (BLBC). BLBC is defined by expression of markers characteristic of basal/myoepithelial cells and is identified as a subgroup of breast cancers that may originate from undifferentiated stem cells (Polyak, 2011). Consistent with this notion, BLBC contains many EMT markers and CSC-like characteristics. We recently showed that Snail interacted with H3K9 methyltransferase G9a and DNA methyltransferase Dnmt1 to silence E-cadherin expression in BLBC cells (Dong et al., 2012). We carried out this study to identify other targets regulated by the Snail-G9a-Dnmt1 complex and investigate their contributions to BLBC.

RESULTS

FBP1 Expression Is Inversely Correlated with Snail in Breast Cancer

To identify potential targets regulated by the Snail-G9a-Dnmt1 complex, we performed microarray analysis in MDA-MB231 cells with knockdown of G9a (GSE34925). Similar to E-cadherin, FBP1 mRNA was greatly elevated after knockdown of G9a. FBP1 has been identified as a marker to distinguish estrogen receptor (ER)-positive breast cancer from ER-negative subtype (van 't Veer et al., 2002). To reveal the potential function of FBP1 in breast cancer, we analyzed FBP1 expression in five gene expression data sets and noticed that FBP1 expression positively correlated with ERα expression (Figure S1A available online). In two data sets (NKI295 and GSE1456) with information on breast cancer subtypes, we found FBP1 expression was high in luminal subtype and significantly lower in BLBC (Figure 1A). Using immunohistochemistry staining, we also found that FBP1 expression positively correlated with ERα expression (Figures 1B and S1B). This correlation was further confirmed using immunoblotting. We found that FBP1 and ERα were highly expressed in luminal subtype but lowly expressed in triple-negative breast cancer, which are mostly also BLBC (Figure S1C; six samples from both cases are shown in Figure 1C). Consistent with the notion that BLBC express EMT molecules, Snail protein level was high in triple-negative breast cancer, and its level inversely correlated with expression of FBP1, ERα, and E-cadherin (Figures 1C and S1C). Furthermore, we examined the expression of FBP1, ERα, and Snail in breast cancer cell lines. BLBC cells lose expression of luminal epithelial molecules (ERα and E-cadherin) and contain high levels of mesenchymal markers (vimentin, N-cadherin, and Snail). Similar to E-cadherin and ERα, FBP1 was high in luminal cell lines and absent in BLBC cell lines (Figure 1D).

FBP1 Is a Direct Target of Snail

To investigate the causal relationship between Snail and FBP1, we expressed Snail in two luminal breast cancer cell lines. Expression of Snail downregulated E-cadherin expression, induced EMT, and converted luminal cells into basal-like phenotype (Dhasarathy et al., 2011) (Figures 2A–2D). This phenotypic conversion is associated with the loss of luminal markers and gain of basal markers (Figures 2D and S2). Similar to E-cadherin, Snail almost completely suppressed FBP1 expression in these cells (Figures 2B–2D). To examine whether FBP1 repression is required for Snail-mediated EMT and basal-like phenotype conversion, Snail was co-expressed with exogenous FBP1 (under the control of CMV promoter and thus not repressed by Snail) in luminal cells (Figure 2A). Ectopic FBP1 expression blocked the downregulation of E-cadherin, inhibited morphological changes indicative of EMT, and suppressed the basal-like phenotype conversion in these cells (Figures 2B, 2D, and S2), indicating that FBP1 repression is required for this event.

We noticed that the FBP1 promoter contained nine consensus Snail-binding E-boxes (CAGGTG) (Figure 2E). We cloned FBP1 promoter (FL1 = −1669 to +331 bp) and generated several deletion mutants of promoter-luciferase constructs based on the location of these E-boxes. By expressing a full-length FBP1 promoter reporter (FL1) in HEK293, HeLa, and MCF7 cells, we found Snail significantly repressed FBP1 promoter activity (Figure 2F). When the E-box at −1273 bp was deleted (FL1 versus FL2), we did not notice any changes in Snail-mediated FBP1 promoter-luciferase repression (Figure 2G), suggesting that the E-box at −1273 is not critical for Snail-mediated FBP1 repression. However, two E-boxes upstream of transcriptional starting site (TSS) (−657 and −358 bp) as well as six consecutive

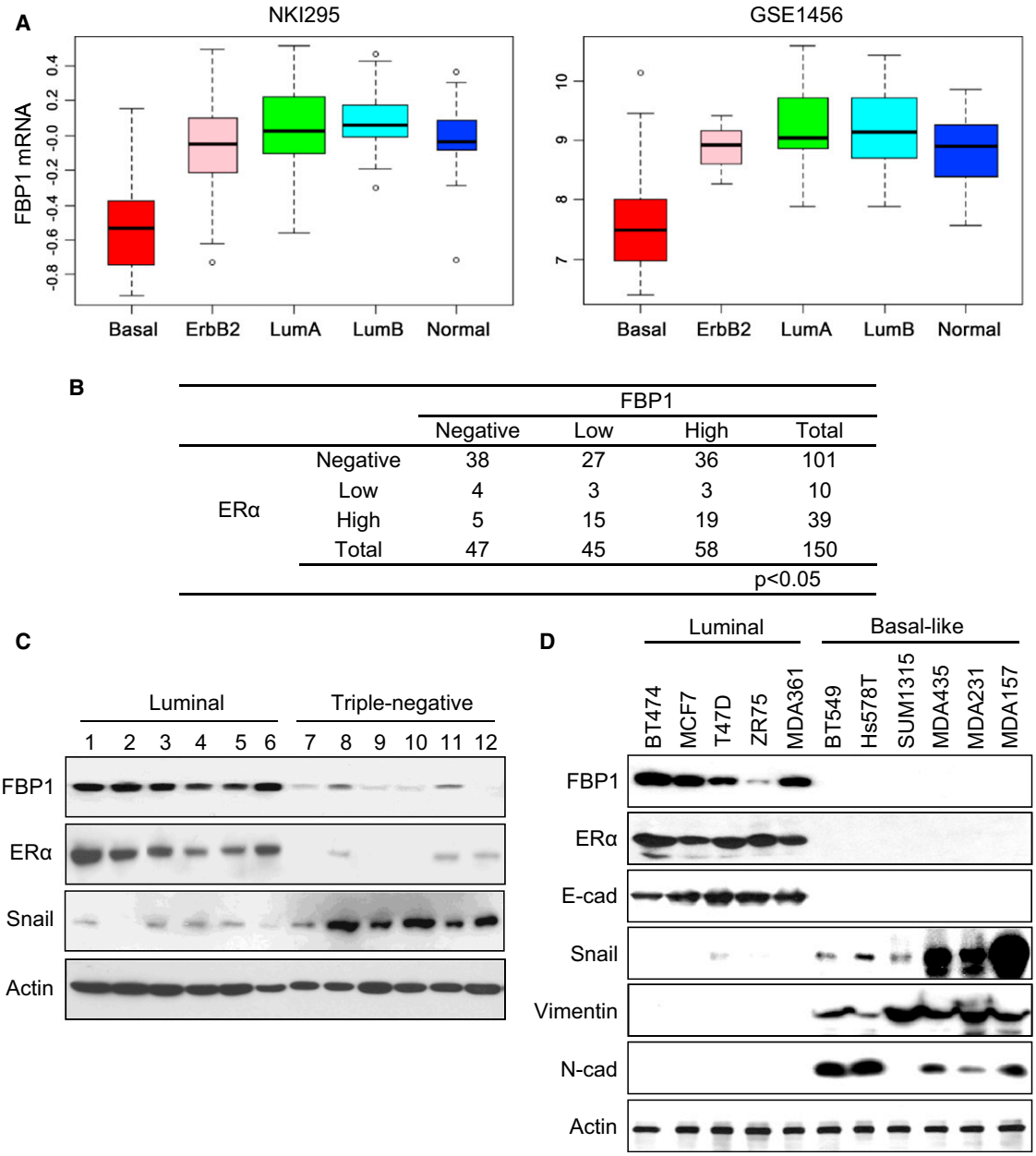

Figure 1. FBP1 Expression Inversely Correlates with Snail in Breast Cancer

(A) Box-plots indicate FBP1 expression in different subtypes of breast cancer.

(B) Statistical analysis of 150 cases of breast tumor samples immunostained using antibodies against FBP1, ER-α, and a control serum.

(C) Expression of FBP1, ER-α, and Snail were analyzed on fresh frozen tumor samples from six cases of luminal and six cases of triple-negative breast cancer.

(D) Expression of FBP1, ER-α, E-cadherin, Snail, and other EMT markers was determined by western blotting on five luminal and six BLBC cell lines (MDA-MB231, MDA-MB435, MDA-MB157, and MDA-MB361 are abbreviated to MDA231, MDA435, MDA157, and MDA361 in all figures).

See also Figure S1.

E-boxes between TSS and ATG sites were important for Snail-mediated FBP1 repression, as deletion constructs (FL3 and FL4) that removed these two regions separately became less sensitive to Snail-mediated repression (Figure 2H). Mutations on these E-boxes almost completely abolished Snail-mediated repression on FBP1 promoter luciferase (Figure 2H).

To examine whether Snail binds to FBP1 promoter, we performed chromatin immunoprecipitation (ChIP) by using three sets of primers (Figure 3A). Primer set 2, which covers nucleotides from −369 to −161, worked effectively and thus was used for the subsequent ChIP experiments. In cells that had undergone Snail-mediated EMT (Figure 2B), we found that Snail was associated with the FBP1 promoter (Figure 3B). In addition, we found endogenous Snail bound to FBP1 promoter in BLBC cells but not luminal cell lines (Figure 3C). These results indicate that FBP1 is a direct target of Snail.

Loss of FBP1 Expression Is Associated with Elevated H3K9me2 and DNA Methylation at the FBP1 Promoter

We hypothesized that the Snail-G9a-Dnmts complex also binds to the FBP1 promoter and is responsible for FBP1 repression in BLBC. In three luminal cell lines that had undergone Snail-mediated EMT, we found that downregulation of FBP1 was associated with an increased G9a and H3K9me2 and decreased H3K9ac at the FBP1 promoter (Figure 3B). We also found FBP1 promoter was completely unmethylated in vector control cell lines; however, de novo DNA methylation occurred at the FBP1 promoter in cells that had undergone Snail-mediated EMT (Figure 3B). The increased G9a association, H3K9me2, and DNA methylation on FBP1 promoter correlated well with the downregulation of FBP1 in these luminal cell lines (Figure 3B).

We also detected a dramatic increase of H3K9me2 and decrease of H3K9ac on the FBP1 promoter in six BLBC cell lines compared to those in five luminal cell lines (Figure 3C). The increase of H3K9me2 at the FBP1 promoter was likely due to the association of the Snail-G9a-Dnmts complex because the occupancy of Snail and G9a at the FBP1 promoter was also significantly higher in BLBC cell lines than in luminal cell lines (Figure 3C). Consistently, all BLBC cell lines showed a significant increase of DNA methylation on the FBP1 promoter, whereas no detectable FBP1 promoter DNA methylation in luminal cell lines was observed (Figure 3C). When analyzing 25 cases of luminal and 16 cases of triple-negative breast tumor tissues (Figure S1C), we found that the association of G9a and the level of H3K9me2 and DNA methylation on the FBP1 promoter were significantly increased in triple-negative breast cancer compared with the luminal subtype (Figure 3D). Knockdown of G9a in MDA-MB231 cells increased the mRNA and protein levels of FBP1 in a way similar to that of E-cadherin (Figure 3E). Knockdown of Snail also increased the expression of FBP1 and E-cadherin in MDA-MB231 cells (Figure S3). Together, these results indicate that the association of Snail and G9a and the corresponding increased H3K9me2 and DNA methylation on FBP1 promoter are critical for the silencing of FBP1 expression in BLBC.

FBP1 Inhibits Glucose Uptake and Sensitivity in BLBC Cells

To examine the function of FBP1 in breast cancer, we established stable clones with FBP1 expression or knockdown in six BLBC and two luminal breast cancer cell lines, respectively (Figure 4A). We first measured glucose uptake and found that FBP1 expression significantly decreased glucose uptake in BLBC cell lines, whereas knockdown of FBP1 enhanced glucose uptake in luminal cell lines (Figure 4B). Intracellular glucose is sensed by MondoA and ChREBP (Li et al., 2006). Following an increase in intracellular glucose-derived metabolites, MondoA and ChREBP shuttle to the nucleus, where they interact with Mlx and activate transcription of target genes. TXNIP is a major direct target of MondoA-Mlx complex and is commonly used as an intracellular glucose sensor (Peterson et al., 2010). We thus examined TXNIP induction by depleting glucose for 12 hr, followed by glucose stimulation for additional 3 hr. TXNIP was robustly induced in BLBC cell lines; however, FBP1 suppressed TXNIP induction. In contrast, knockdown of FBP1 stimulated TXNIP induction in luminal cells (Figure 4C). Because the cells had been glucose-deprived for 12 hr, the TXNIP levels were re-set to baseline (lane 2 versus lane 1, Figure S4A); the induction of TXNIP after glucose stimulation reflects glucose uptake and resultant steady-state level of intracellular glucose. Indeed, following glucose stimulation for different time intervals, TXNIP induction was greatly delayed in FBP1-expressing MDA-MB231 cells. In contrast, TXNIP induction was robustly increased in FBP1-knockdown MCF7 cells (Figure S4A). Because insulin is the major hormone regulating glucose uptake, we measured insulin sensitivity by examining tyrosine phosphorylation of the insulin receptor (IR) after insulin stimulation. We found that FBP1 expression suppressed the intensity and duration of IR phosphorylation in BLBC cell lines. Conversely, knockdown of FBP1 increased the intensity and duration of IR phosphorylation in luminal cell lines (Figure S4B). These results indicate that FBP1 is critical in inhibiting glucose uptake exemplified by downregulating glucose and insulin sensitivities.

FBP1 Reduces Lactate Generation and Increases Oxygen Consumption in BLBC Cells

To examine whether FBP1 changes glucose metabolism from aerobic glycolysis to OXPHOS, we measured lactate production and found that FBP1-expressing BLBC cells produced less lactate than their vector control cells, whereas FBP1-knockdown luminal cells had more lactate production (Figure 4D). We then investigated FBP1's role on cell growth under different oxygen conditions. At normoxic condition (21% oxygen), FBP1 expression induced a minor inhibition in cell growth in BLBC cell lines. Similarly, knockdown of FBP1 did not cause an apparent effect on the growth of luminal cells (Figure S4C). However, under hypoxic condition (0.1% oxygen), FBP1 expression induced a drastic growth inhibition in BLBC cell lines, whereas knockdown of FBP1 significantly reduced hypoxia-mediated growth inhibition in luminal cell lines (Figure 4E), suggesting that the effect of FBP1 on cell growth depends on oxygen. We thus examined oxygen consumption rate (OCR). We found that the basal OCR significantly increased in FBP1-expressing BLBC cells, whereas FBP1-knockdown luminal cells displayed a decrease in basal OCR (Figure 4F). Similar results were obtained in the analysis of ATP-linked and maximal OCR (Figure 4F).

FBP1 Inhibits Glycolysis and Increases OXPHOS

For every glucose molecule a cell consumes, aerobic glycolysis produces 2 ATP, whereas OXPHOS produces 36 ATP. We found that FBP1 expression or knockdown did not alter the steady-state level of ATP in BLBC or luminal cells under normoxic condition (Figure S5A). However, under hypoxia, the steady-state level of ATP was significantly decreased in FBP1-expressing BLBC cells, whereas knockdown of FBP1 greatly reduced hypoxia-mediated ATP reduction in luminal cells (Figure S5A). Consistent with these observations, oligomycin treatment resulted in a significant growth inhibition in FBP1-expressing BLBC cells. Conversely, knockdown of FBP1 provided luminal cells with resistance to this compound (Figure S5B). Although BLBC cell lines are less sensitive to growth inhibition mediated by hypoxia or oligomycin compared with their FBP1-expressing clones, they were extremely sensitive to glucose deprivation, as indicated by massive cell death and

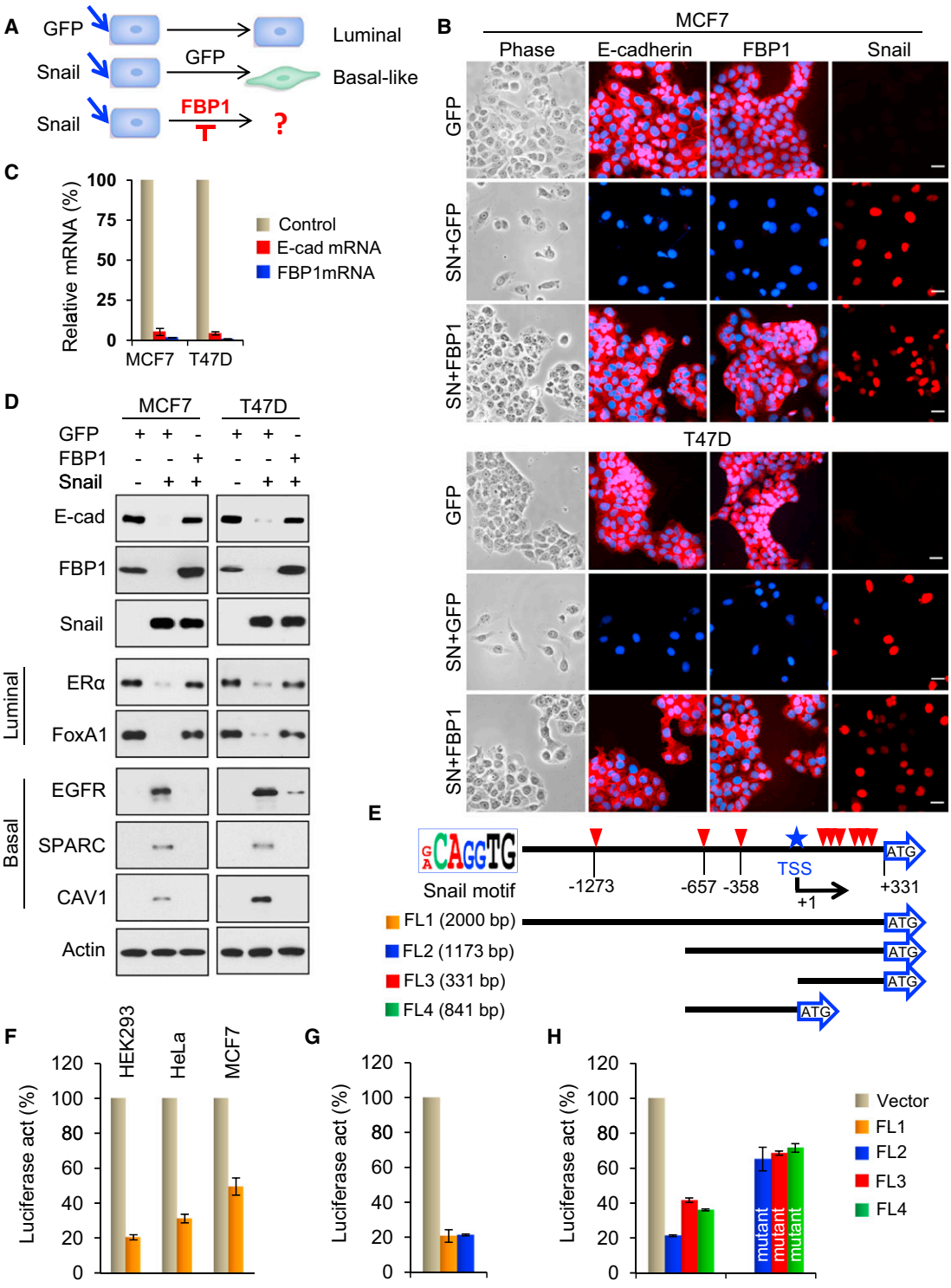

Figure 2. Snail Represses FBP1 Expression

(A) Schematic diagram showing that Snail was coexpressed with vector (GFP) or FBP1 (CMV promoter) in luminal subtype breast tumor cells.

(B) Snail was coexpressed with vector (GFP) or FBP1 in MCF7 and T47D cells for 4 days. Morphologic changes indicative of EMT are shown in the phase contrast images; expression of FBP1 and E-cadherin were analyzed by immunofluorescent staining. Nuclei were visualized with DAPI (blue). Scale bar = 20 μm.

(C) The mRNA levels of E-cadherin and FBP1 were quantitated by real-time PCR (mean ± SD in three separate experiments).

(D) Expression of E-cadherin, FBP1, Snail, luminal markers (ER-α and FoxA1), and basal markers (EGFR, SPARC, and Caveolin-1) for cells in (B) was analyzed by western blotting.

(E) Schematic diagram showing positions of nine potential Snail-binding E-boxes on the FBP1 promoter and FBP1 promoter luciferase construct used.

(legend continued on next page)

detachment from the cell substratum after 48 hr of glucose depletion (Figure S5C).

We further investigated the metabolic fate of [U-^{13}C]-glucose in vector- and FBP1-expressing MDA-MB231 cells by using stable isotope-resolved metabolomics (SIRM) (Fan et al., 2009; Fan et al., 2011; Le et al., 2012). Nuclear magnetic resonance (NMR) analysis of the culture media demonstrated a reduced $^{13}C_6$-glucose uptake and $^{13}C_3$-lactate excretion, leading to an overall decrease of $^{13}C_6$-glucose to $^{13}C_3$-lactate conversion in FBP1-expressing cells (Figures 5A and S5D). NMR analysis of ^{13}C-labeled metabolites in cell extracts also indicated a reduced $^{13}C_3$-lactate in FBP1-expressing cells (Figure 5B), consisting of reduced $^{13}C_3$-lactate excretion into the media. Interestingly, FBP1 expression also reduced ^{13}C abundance in the ribosyl unit of ribonucleotides and derivatives (i.e., AXP, UXP, NAD^+, and UDPG) (Figure 5B), suggesting that the pentose phosphate pathway (PPP), which is responsible for generating ribose-5-phosphate for the synthesis of ribonucleotides and NADPH production, is inhibited. In line with this finding, the ratio of $NADP^+$/NADPH was increased in FBP1-expressing MDA-MB231 cells, whereas this ratio was decreased in FBP1-knockdown MCF7 cells (Figure S5E). The decreased level of ^{13}C-UDPG in FBP1-expressing cells suggests that the glycosylation process is reduced. The same cell extracts were further analyzed by GC-MS to quantify ^{13}C-metabolites involved in glycolysis and the TCA cycle (Figure 5C). We found that the production of the m3 or $^{13}C_3$-isotopologues of glycerol-3-phosphate (G3P) and serine were significantly reduced in FBP1-expresing cells, which is again consistent with attenuated glycolytic activity. In line with the observations that FBP1 increased OXPHOS, the production of $^{13}C_2$ or m2-succinate, fumarate, and malate (markers of the first turn of the TCA cycle) as well as the $^{13}C_4$- or m4-citrate (markers of the second turn of the TCA cycle) (Fan et al., 2010) were increased in FBP1-expressing cells (Figure 5C). Together, these results indicate that FBP1 inhibits glycolytic flux, reduces biosynthesis (nucleotides via PPP, G3P for triacylglycerol synthesis, and serine for protein), and enhances OXPHOS.

FBP1 Suppresses PKM2 Activation and Increases Mitochondrial Complex I Activity and Reactive Oxygen Species Generation

To explore the underlying mechanisms of increased OXPHOS by FBP1, we first assessed the level of F-1,6-BP. FBP1 expression caused a dramatic decrease of F-1,6-BP level in BLBC cells, whereas knockdown of FBP1 led to a marked increase of F-1,6-BP in luminal cell lines (Figure 6A). We also measured pyruvate kinase (PK) activity and found that FBP1 significantly decreased PK activity in two BLBC cell lines; whereas knockdown of FBP1 increased PK activity in two luminal cells (Figure S6A). The PK activity contained both PKM1 and PKM2 activities and thus we could not distinguish the activation of PKM2 by F-1,6-BP. We next examined the tetrameric form of PKM2 using cross-linking agent. Surprisingly, PKM2 existed mainly in tetrameric form in two BLBC cell lines, whereas it appeared in monomer state in two luminal cell lines (Figure 6B). FBP1 expression significantly decreased the tetrameric PKM2, whereas knockdown of FBP1 increased the formation of tetrameric PKM2. These data indicate that loss of FBP1 activates PKM2, which facilitates lactate production and triggers the switch to aerobic glycolysis.

Because FBP1 expression enhanced oxygen consumption, we reasoned that FBP1 expression stimulates activity in the mitochondrial electron transport complexes (I, II, III, and IV of ETC) (Figure 6C). Complexes I and II use electrons donated from NADH and FADH2, respectively, to reduce coenzyme Q, which shuttles these electrons to complex III, where they are transferred to cytochrome c. Complex IV uses electrons from cytochrome c to reduce molecular oxygen to water. These actions produce a proton electrochemical potential gradient, and the free energy released is converted to ATP by ATP synthase (Chatterjee et al., 2011). We first compared the activity of the mitochondrial complexes I and II in terms of their contribution to the overall oxygen consumption. Complex I and II activity could be blocked by rotenone and TTFA, respectively, thus the oxygen consumption relies on the electron transport activity of the remaining active complex. As shown in Figure 6C, although OCR was higher in FBP1-expressing BLBC cell lines, addition of TTFA slightly and proportionally decreased OCR in both vector- and FBP1-expressing BLBC cells. A consistent trend was observed in vector- and FBP1-knockdown luminal cell lines (Figure 6C). However, treatment with rotenone dramatically reduced OCR in FBP1-expressing BLBC cells to levels found in vector control cells (Figure 6C). Consistently, treatment with rotenone also decreased OCR in luminal cells to levels similar to those found in the FBP1-knockdown luminal cells. We also measured complex I activity using purified mitochondria from these cells. FBP1-expressing BLBC cell lines had significant higher complex I activity, whereas FBP1-knockdown luminal cell lines had decreased complex I activity (Figure 6D). To identify the underlying mechanism, we performed microarray analysis (GSE41158) and determined that mitochondrial transcription factor B1M (TFB1M) was significantly higher in FBP1-expressing BLBC cells (Figure S6B). TFB1M is a nuclear gene encoding mitochondrial transcription factor that is essential for the mitochondrial biogenesis (Metodiev et al., 2009). Loss of TFB1M causes defects of protein translation in mitochondrial complex I components, resulting in impaired OXPHOS (Koeck et al., 2011). We found that TFB1M expression was increased in FBP1-expressing MDA-MB231 cells, whereas its expression was decreased in FBP1-knockdown MCF7 cells (Figures S6B and S6C). In addition, two targets of TFB1M from mitochondrial complex I, ND1 and ND5, but not components from complex

(F) FBP1 promoter luciferase construct (FL1) was coexpressed with Snail or vector in HEK293, HeLa, and MCF7 cells, respectively. After 48 hr, luciferase activities were determined and normalized (mean ± SD in three separate experiments).
(G) FBP1 promoter luciferase constructs (FL1 and FL2) were coexpressed with Snail or vector in HEK293 cells. Luciferase activities were determined as in (F).
(H) FBP1 promoter luciferase constructs (FL2, FL3, and FL4 as well as their E-box mutants) were coexpressed with Snail or vector in HEK293 cells. Luciferase activities were determined as in (F).
See also Figure S2.

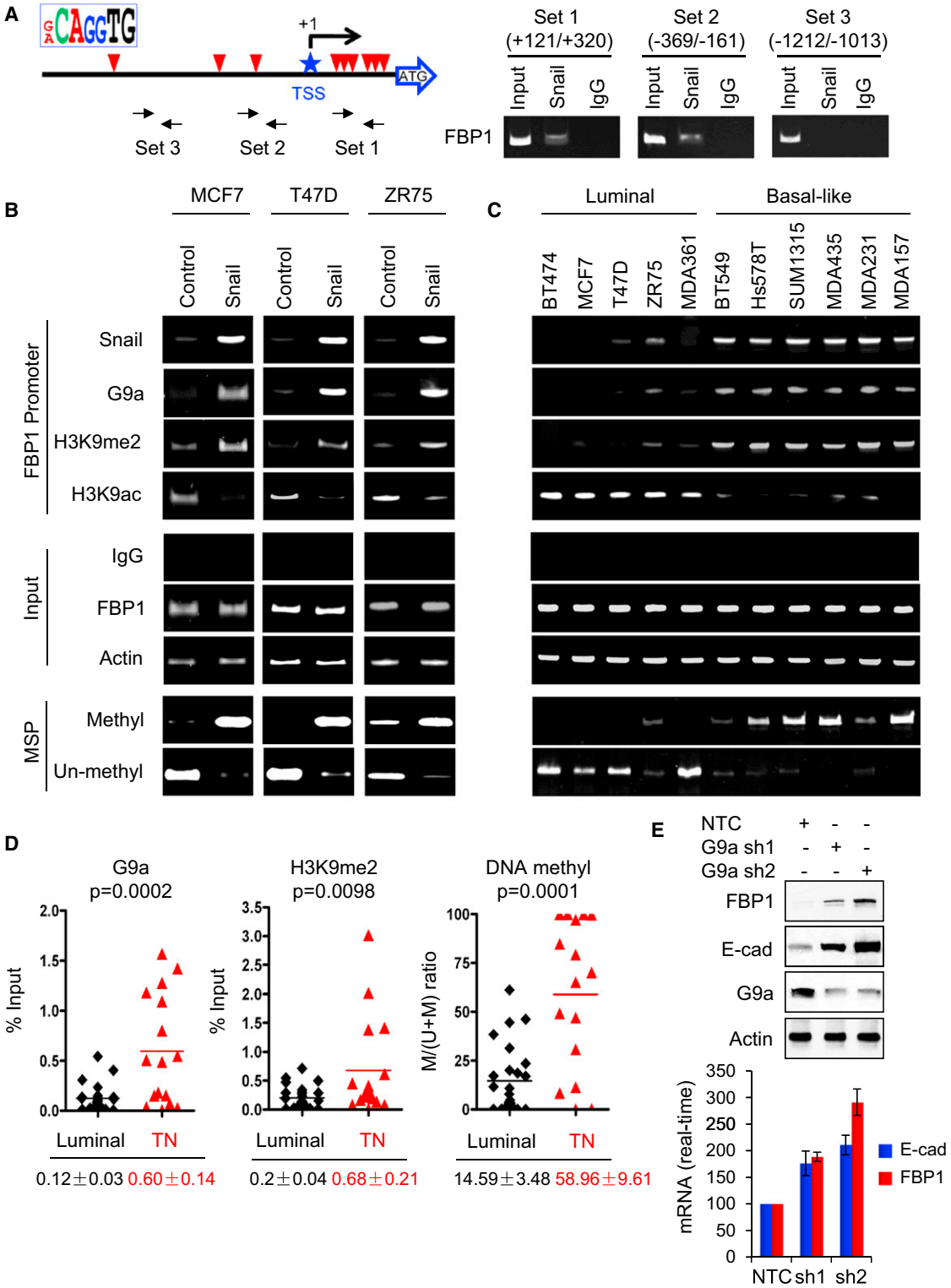

Figure 3. Snail and G9a Are Required for H3K9me2 and DNA Methylation at the FBP1 Promoter

(A) Three sets of primers used for FBP1 promoter ChIP are shown.

(B and C) The association of Snail and G9a, and the level of H3K9me2 and H3K9ac at the FBP1 promoter in cells that have undergone Snail-mediated EMT (B) and cell lines from Figure 1D (C) were analyzed by ChIP. DNA methylation at the FBP1 promoter was analyzed by MSP.

(D) The association of G9a, and the level of H3K9me2 and DNA methylation at the FBP1 promoter in luminal (25 cases) and triple-negative (16 cases) breast cancer tissues were analyzed by ChIP and MSP, respectively. Horizontal lines represent mean values. Statistical analyses (mean ± SD in three separate experiments) are shown below.

(legend continued on next page)

II-IV were also elevated in FBP1-expressing cells. Together, these data indicate that the rise of complex I activity is the main factor underlying the increase of mitochondrial oxygen consumption in FBP1-expressing cells.

In ETC, a small percentage of electrons are prematurely leaked to oxygen, mainly from complex I and/or complex III, forming the majority of reactive oxygen species (ROS; Chatterjee et al., 2011). To test whether an increase in mitochondrial OCR and complex I activity by FBP1 would accompany an increase of ROS, we examined intracellular ROS levels using CellROX deep red. FBP1-expressing BLBC cells showed a substantial increase in ROS levels, whereas FBP1-knockdown luminal cell lines induced a significant decrease of ROS (Figures 6E and 6F). A similar finding was observed for superoxide production using Mito-Sox Red and DHE staining (Figure S6D). These data indicate that FBP1 expression contributes to the increase of cellular ROS.

FBP1 Suppresses CSCs and Inhibits Tumorigenicity of Breast Cancer

To examine whether FBP1 expression alters CSC characteristics of BLBC, we examined tumorsphere formation of these cells under normoxic and hypoxic conditions. FBP1 expression greatly suppressed tumorsphere formation in BLBC cell lines (Figure 7A), and this inhibitory effect was enhanced by hypoxia (Figure S7A). Conversely, knockdown of FBP1 in luminal cell lines enhanced tumorsphere formation in normoxic condition, and this effect was also substantiated under hypoxia.

Breast CSCs are enriched in cells with a $CD44^{high}/CD24^{low}/EpCAM^{+}$ phenotype (Blick et al., 2010). We found that FBP1 expression significantly reduced the percentage of $CD44^{high}/CD24^{low}/EpCAM^{+}$ population in BLBC cell lines (Figures 7B and 7C). Conversely, knockdown of FBP1 induced a significant increase of $CD44^{high}/CD24^{low}/EpCAM^{+}$ population in luminal cell lines. Because CD44 is a known target of β-catenin, and because activation of β-catenin is often found in BLBC (DiMeo et al., 2009; Zeilstra et al., 2008), we reasoned that the elevated ROS caused by FBP1 expression compromises β-catenin activity. In the cellular aging process, ROS antagonizes β-catenin activity by shifting the interaction of β-catenin with TCF4 toward FOXO3a (Figure 7D) (Bowerman, 2005; Essers et al., 2005; Manolagas and Almeida, 2007). We found that β-catenin interacted with TCF4 in BLBC cells. However, the interaction of β-catenin with TCF4 was significantly decreased and substituted with an increased interaction of β-catenin with FOXO3a in FBP1-expressing cells (Figure 7E). Similarly, knockdown of FBP1 in luminal cells increased the interaction of β-catenin with TCF4. The differential interactions of β-catenin with TCF4 were consistent with the luciferase reporter assays showing that FBP1-expressing cells had lower TOP-Flash and higher FOXO3a luciferase activities than vector control cells (Figure S7B). In addition, expression of several target genes of β-catenin (Axin2, CD44, and ID2) and FOXO3a (CDKN2A and SOD2) were in line with these binding and promoter luciferase assays (Figure S7C). Consistently, NAC treatment restored the interaction of β-catenin with TCF4 as well as their luciferase activities and target gene expression (Figures 7E, S7B, and S7C). In addition, treatment with NAC and EUK134 restored tumorsphere formation in FBP1-expressing BLBC cells (Figure S7D).

We also measured the in vitro tumorigenicity of these cells using soft-agar assay. Although BT549 and SUM1315 cells could not form colonies, the other FBP1-expressing BLBC cell lines had significantly fewer colonies than their corresponding vector controls; whereas knockdown of FBP1 increased colony formation in luminal cell lines (Figure 8A). NAC treatment restored colony growth in FBP1-expressing BLBC cells, indicating that the elevated ROS impairs their tumorigenicity in vitro (Figure S8A). To examine the tumorigenicity in vivo, we injected mammary fat pads of SCID mice with the following three pairs of cell lines: (1) vector- and FBP1-expressing MDA-MB231 cells, (2) vector- and FBP1-expressing MDA-MB435 cells, and (3) vector- and FBP1-knockdown MCF7 cells. As shown in Figure 8B, FBP1-expressing MDA-MB231 cells failed to form tumors in all six mice. Similarly, tumors derived from FBP1-expressing MDA-MB435 cells had a significantly reduced tumor size compared with vector control cells. In line with these findings, FBP1-knockdown MCF7 cells showed significantly enhanced tumor growth compared with vector control cells (Figure 8B). Strikingly, NAC treatment greatly increased tumor formation in FBP1-expressing MDA-MB231 and MDA-MB435 cells (Figures S8B and S8C). Together, these data indicate that FBP1 expression increases ROS production, which compromises CSC properties by shifting the interaction of β-catenin from TCF4 to FOXO3a, and thus inhibits tumorigenicity in vitro and tumor formation in vivo.

We then examined the correlation of FBP1 expression with patient survival in NKI295 that consists of 295 patients with node-negative breast cancer (van de Vijver et al., 2002). Expression of FBP1 can separate patients into two prognostic groups, with high FBP1 expression having a better survival rate (Figure 8C). This clinical validation supports the finding that FBP1 repression is critical in EMT and BLBC.

DISCUSSION

Our study provides several insights into EMT and breast cancer. First, loss of FBP1 is essential to trigger glycolytic reprogramming and results in several metabolic benefits in BLBC: (1) increase glucose uptake and sensitivity as evidenced by elevated TXNIP and IR phosphorylation after stimulation, (2) increased glycolytic intermediates for biosynthesis (such as PPP, glycerol-3-phosphate, and serine), (3) maintenance of ATP production under hypoxia, and (4) reduced oxygen dependence and ROS production (Figure 8D). These observations are consistent with the notion that FBP1 deficiency causes hypoglycemia and acidosis in patients and that inhibition of FBP1 restores glucose uptake in the type 2 diabetic model.

(E) Expression of FBP1 and E-cadherin was examined in MDA-MB231 cells with knockdown of G9a expression (top panel). Their mRNA levels were also quantified by real-time PCR (bottom panel). Data are presented as a percentage of non-target control (NTC) values (mean ± SD in three separate experiments in duplicates).
See also Figure S3.

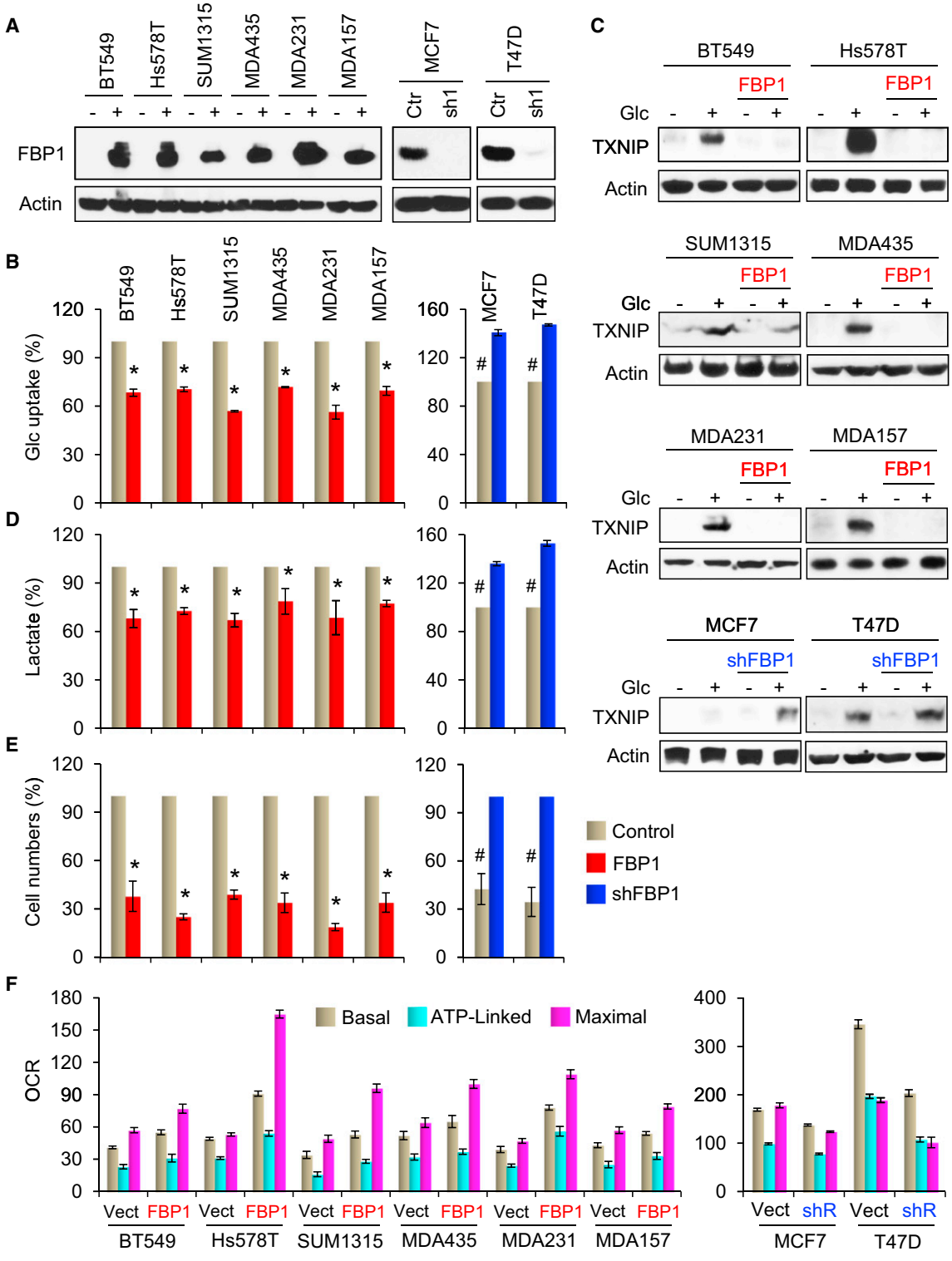

Figure 4. FBP1 Inhibits Glucose Uptake and Sensitivity and Suppresses Cell Growth under Hypoxia

(A) Stable clones with FBP1 expression or knockdown were established in six BLBC and two luminal cell lines, respectively.

(B) Glucose uptake was measured.

(C) Cells were deprived for glucose for 12 hr followed by glucose stimulation for additional 3 hr. TXNIP expression was examined by western blotting.

(D) Lactate excretion was measured.

(E) Cell growth under hypoxic condition was measured by cell-count assay for 2 days. Data are presented as a percentage of vector control values for BLBC cells, whereas data are presented as a percentage of FBP1-knockdown groups for luminal cells (mean ± SD in three separate experiments in triplicates).

(legend continued on next page)

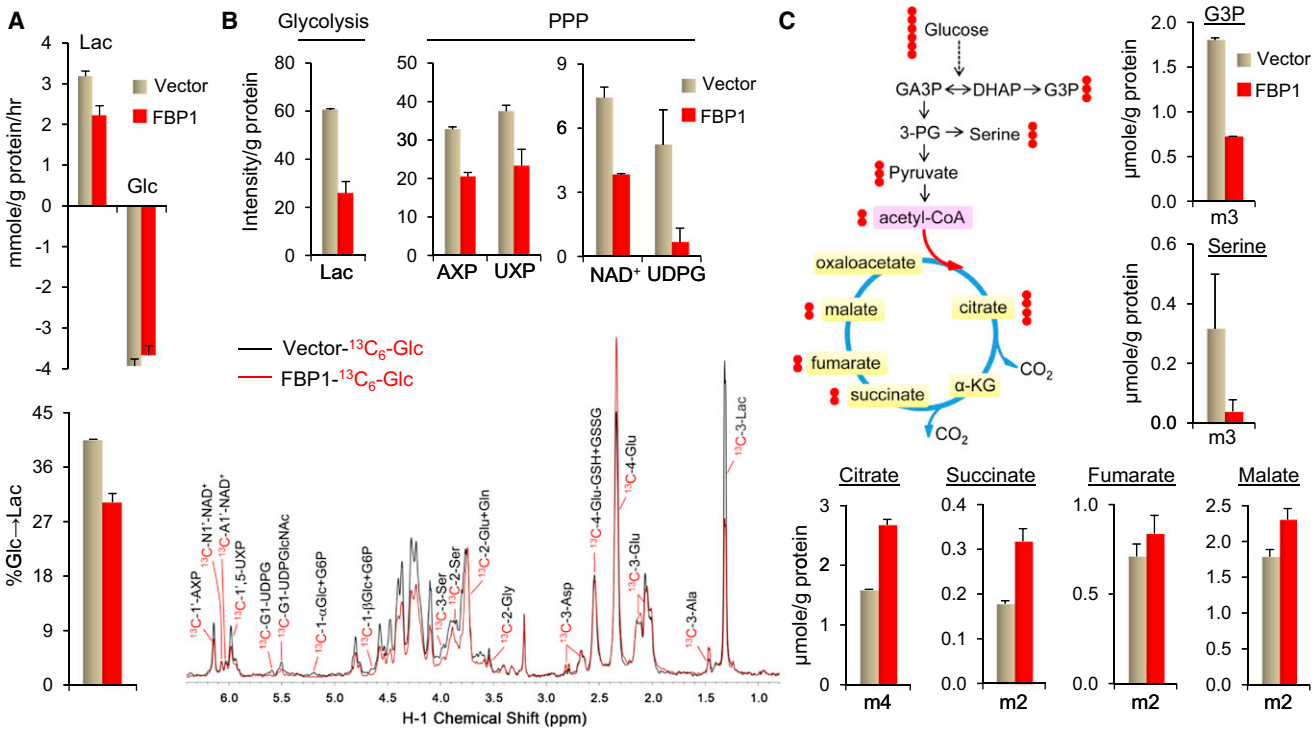

Figure 5. FBP1 Inhibits Glycolysis and Increases OXPHOS

(A) $^{13}C_6$-Glucose uptake, $^{13}C_3$-lactate production, and the conversion of $^{13}C_6$-Glucose to $^{13}C_3$-lactate were measured by 1D ^{1}H NMR analysis of the media of vector- and FBP1-expressing MDA-MB231 cells grown in $^{13}C_6$-Glucose (mean ± SEM in duplicate). ^{1}H NMR spectra from the media are shown in Figure S5D.

(B) A pair of representative 1D ^{1}H{^{13}C} HSQC NMR spectra show the changes in ^{13}C abundance (represented by the intensity of ^{13}C-attached ^{1}H peaks) of various assigned metabolites elicited by FBP1 expression in MDA-MB231 cells (black, control vector; red, FBP1, bottom panel). The relative ^{13}C abundance of indicated metabolites from cell extracts was quantified from their HSQC peak intensity (Fan and Lane, 2008) (mean ± SEM in duplicate). Lac, lactate; AXP, adenine nucleotides; UXP, uracil nucleotides; UDPG, UDP-glucose.

(C) Top left panel shows the expected ^{13}C (●) labeling patterns of glycolytic and TCA cycle metabolites with $^{13}C_6$-Glc as tracer. The doubly ^{13}C labeled TCA cycle metabolites are derived from the first turn of the TCA cycle while the quadruply ^{13}C labeled citrate is produced from the second turn of the cycle. The levels of several indicated ^{13}C isotopologues of glycolytic and TCA cycle metabolites were obtained from the GC-MS analysis of the same cell extracts as in (B) (mean ± SEM in duplicate).

See also Figure S5.

The activity of PKM2 oscillates between the activated tetrameric form and inactivated monomeric state, which constitutes the metabolic budget system in tumor metabolism (Mazurek et al., 2005). F-1,6-BP increases the formation of tetrameric PKM2. Glucose is then fueled to lactate along with ATP production until F-1,6-BP levels drop below a minimum signal level, which causes the disassembly of the tetrameric PKM2 into a monomeric state. We found that PKM2 mainly existed in tetrameric form in BLBC cells and existed predominantly in a monomeric state in luminal cells. This observation corresponds with the findings that BLBC cells contain a high level of F-1,6-BP, an increased PK activity, and increased lactate production. FBP1 expression significantly decreased the formation of tetrameric PKM2 in BLBC cells by reducing F-1,6-BP. Because the major function of glycolysis is to provide high levels of glycolytic intermediates for biomass synthesis, we speculate that two modes of PKM2 are used in glycolysis. The first mode is the inhibition of PKM2 (economic mode), which blocks glycolytic flux for accumulation of intermediates required for biosynthesis. The second mode is the overall increase of glycolytic flux with activation of PKM2 (luxury mode). The rise of intermediates results not from a block of PKM2, but from an increased load of glycolysis through glucose (Figure 8D). As pointed out by Vander Heiden and colleagues, although this seems wasteful, it ensures that the glycolytic intermediates will not be depleted and maintain precursor concentrations at constant and ample levels for allowing maximum biosynthesis during rapid cell growth (Lunt and Vander Heiden, 2011). Our study indicates that BLBC cells employ the luxury mode of glycolysis by suppressing FBP1 for increasing glucose assimilation and rapid channeling of glycolytic intermediates in biosynthesis at the cost of host.

PKM2 is the main enzyme for ATP production in glycolysis. This inefficient but faster mode of ATP production may be

(F) Oxygen consumption was measured (mean ± SD in three separate experiments in triplicate).

For B and D, data are presented as a percentage of vector control values (mean ± SD in three separate experiments in triplicates). For B, D, and E, *$p < 0.01$ and #$p < 0.01$ for vector control cells compared with their FBP1-expressing or FBP1-knockdown clones, respectively.

See also Figure S4.

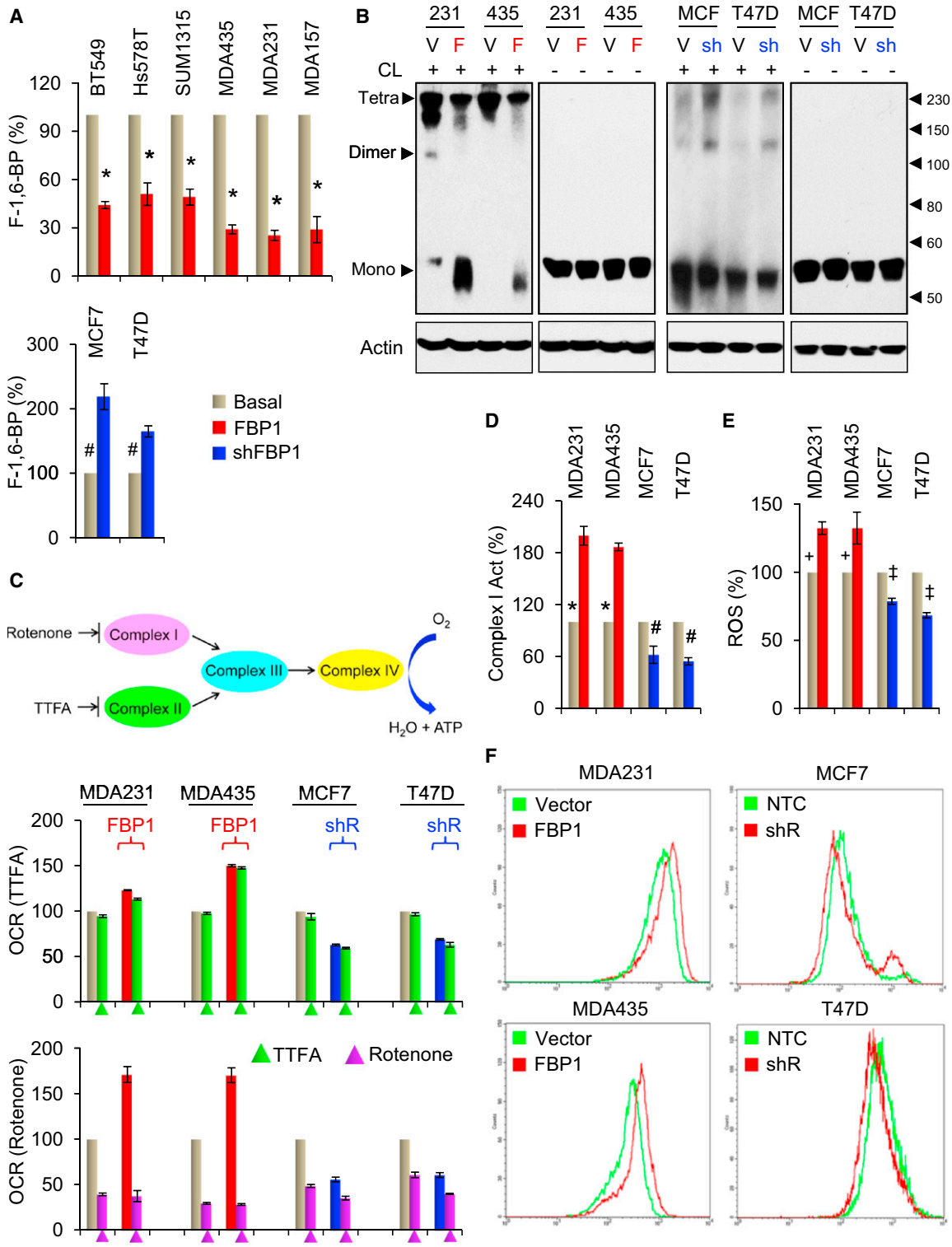

Figure 6. FBP1 Suppresses PKM2 Activation and Increases Complex I Activity and ROS Production

(A) F-1,6-BP was measured in FBP1-expressing and FBP1-knockdown clones.

(B) Cells were either treated with (+) or without (−) 1% formaldehyde (crosslinker; CL) for 20 min immediately after cell lysis. The states of monomer, dimer, and tetramer of PKM2 were analyzed by western blotting.

(C) Schematic diagram showing the electron transfer from mitochondrial complex I to IV. Cells were treated with Rotenone and TTFA, respectively. Oxygen consumption was measured (mean ± SD in three separate experiments in triplicate).

(D) Complex I activity was measured from mitochondria isolated from cells in (C).

(legend continued on next page)

preferred to meet the cellular demands of BLBC, particularly under hypoxic condition. Under hypoxia, the steady-state level of ATP in BLBC cells declined slightly; however, FBP1 expression resulted in a dramatic plunge in ATP level. This is in line with the observation that BLBC cells are less sensitive to growth inhibition under hypoxia or by oligomycin. Given that BLBC cells are highly invasive, this metabolic switch empowers them to absorb glucose and maintain ATP level in a nutrient-poor and hypoxic condition. In addition, the acidic microenvironment created by excreted lactate facilitates the degradation of extracellular matrix and protects BLBC cells from inhibition by an immune response at the metastatic site (Figure 8D).

The phenomenon during which increased glucose uptake and exacerbated glycolytic activity often accompany OXPHOS inhibition is known as a Crabtree effect and had been identified in tumors and other mitotically active tissues (Crabtree, 1929). We found that the inhibition of complex I activity is mainly responsible for the Crabtree effect in BLBC cells. Expression of FBP1 significantly increased mitochondrial complex I activity by inducing the expression of TFB1M, which is required for the translation of ND1 and ND5 of mitochondrial complex I (Koeck et al., 2011). These data provide mechanistic insights and support our finding that loss of FBP1 suppresses OXPHOS in BLBC cells.

Second, our results indicate that the glycolytic switch enhances CSC characteristics in BLBC by reducing ROS. It has been noted that somatic cells primarily utilize OXPHOS for their energy production, whereas pluripotent cells rely on glycolysis (Facucho-Oliveira and St John, 2009). Using an iPSC as a model in stem cell reprogramming, mitochondria were found to change from a mature cristae-rich morphology in somatic cells to more immature spherical and cristae-poor structures in iPSCs. Intriguingly, the glycolytic change occurs in cells prior to their acquisition of pluripotent markers, suggesting that the glycolytic switch plays a causative role in the iPSC reprogramming rather than simply being a consequence of acquiring pluripotency. The induction of pluripotency with a glycolytic switch is consistent with the observation that a hypoxic environment maintains the stem cell state and hypoxia facilitates the reprogramming process (Mohyeldin et al., 2010). In the stem cell niche, protection from ROS is critical for the maintenance of self-renewal of hematopoietic stem cells and human and mouse breast CSCs (Diehn et al., 2009). These observations indicate that the self-renewal potential of CSCs is exquisitely sensitive to the level of ROS. We found that FBP1-expressing BLBC cells increased OXPHOS and ROS production. The increased ROS was associated with the suppression of tumorsphere and decreased CSC markers ($CD44^{high}/CD24^{low}/EpCAM^{+}$). In addition, FBP1 expression in BLBC cells inhibited tumorigenicity in vitro and suppressed tumor formation in vivo. Mechanistically, elevated ROS shifts the interaction of β-catenin from TCF4 to FOXO3a and thus compromises β-catenin activity, which is essential for the maintenance of pluripotency. NAC treatment returns the interaction of β-catenin with TCF4 and restores tumorigenicity in vitro and in vivo. Together, these data indicate that the loss of FBP1 greatly increases CSC traits by repressing ROS production and maintaining the interaction of β-catenin with TCF4 in BLBC.

Third, our study indicates that FBP1 is a major downstream target of Snail in controlling glycolysis. We identified that the Snail-G9a-Dnmt1 complex, which is required for E-cadherin silencing, is responsible for FBP1 repression in BLBC. FBP1 silencing is required for Snail-mediated EMT and the conversion from luminal to basal-like phenotype in breast cancer. In addition, knockdown of Snail or G9a restores the expression of E-cadherin and FBP1. Our results indicate that this metabolic reprogramming (resulting from the loss of FBP1) synergizes with the loss of E-cadherin to sustain CSC-like properties during dissemination and metastasis. Our study strengthens the notion that metabolic reprogramming is inextricably intertwined with tumorigenesis and fortifies Warburg's historical claim that metabolism is an actionable event instead of an accompanied biomarker in oncogenesis (Ward and Thompson, 2012). Our study also reveals that the Snail-mediated epigenetic regulation may represent the Achilles' heel of BLBC. Thus, targeting this chromatin modification complex will generate an entirely effective approach for treating metastatic breast cancer.

EXPERIMENTAL PROCEDURES

Plasmids, siRNA, and Antibodies

FBP1 shRNA was purchased from MISSION shRNA at Sigma-Aldrich (St Louis, MO). Human FBP1 was amplified from a HeLa cDNA library and subcloned into pLenti6.3. Antibody information is provided in the Supplemental Experimental Procedures.

Cell Culture

Breast cancer cell lines were cultured as described previously (Dong et al., 2012). For establishing stable transfectants with expression or knockdown of FBP1, BLBC cells and luminal cells were transfected with pLenti6.3/FBP1 and FBP1 shRNA, respectively; stable clones were selected with puromycin (300 ng/ml) for 4 weeks.

Immunostaining, Immunoprecipitation, Immunoblotting, Immunohistochemical Staining

All protocols are described in detail in the Supplemental Experimental Procedures.

Human Breast Tumors

The frozen fresh tumor samples were collected from resected breast tumors from patients at the University of Texas MD Anderson Cancer Center with informed consent and institutional IRB approval. These frozen samples were snap-frozen in liquid nitrogen and stored at −80°C. Data regarding the stage, grade, and expression of ER-α, PR, and HER2 are described previously (Dong et al., 2012).

Metabolic Assays

Glucose uptake, lactate production, ATP levels, and PK activity were measured by assay kits from BioVision (San Francisco, CA). Oxygen consumption was determined using the Seahorse Extracellular Flux (XF-96)

(E and F) ROS generation was analyzed by flow cytometry (mean ± SD in three separate experiments in duplicates). Representative images are shown (F). $^{+}p < 0.05$ and $^{‡}p < 0.05$ for vector control cells compared with their FBP1-expressing or FBP1-knockdown clones, respectively.
For A and D, data are presented as a percentage of vector control values (mean ± SD in three separate experiments in triplicates). $^{*}p < 0.01$ and $\#p < 0.01$ for vector control cells compared with their FBP1-expressing or FBP1-knockdown clones, respectively.
See also Figure S6.

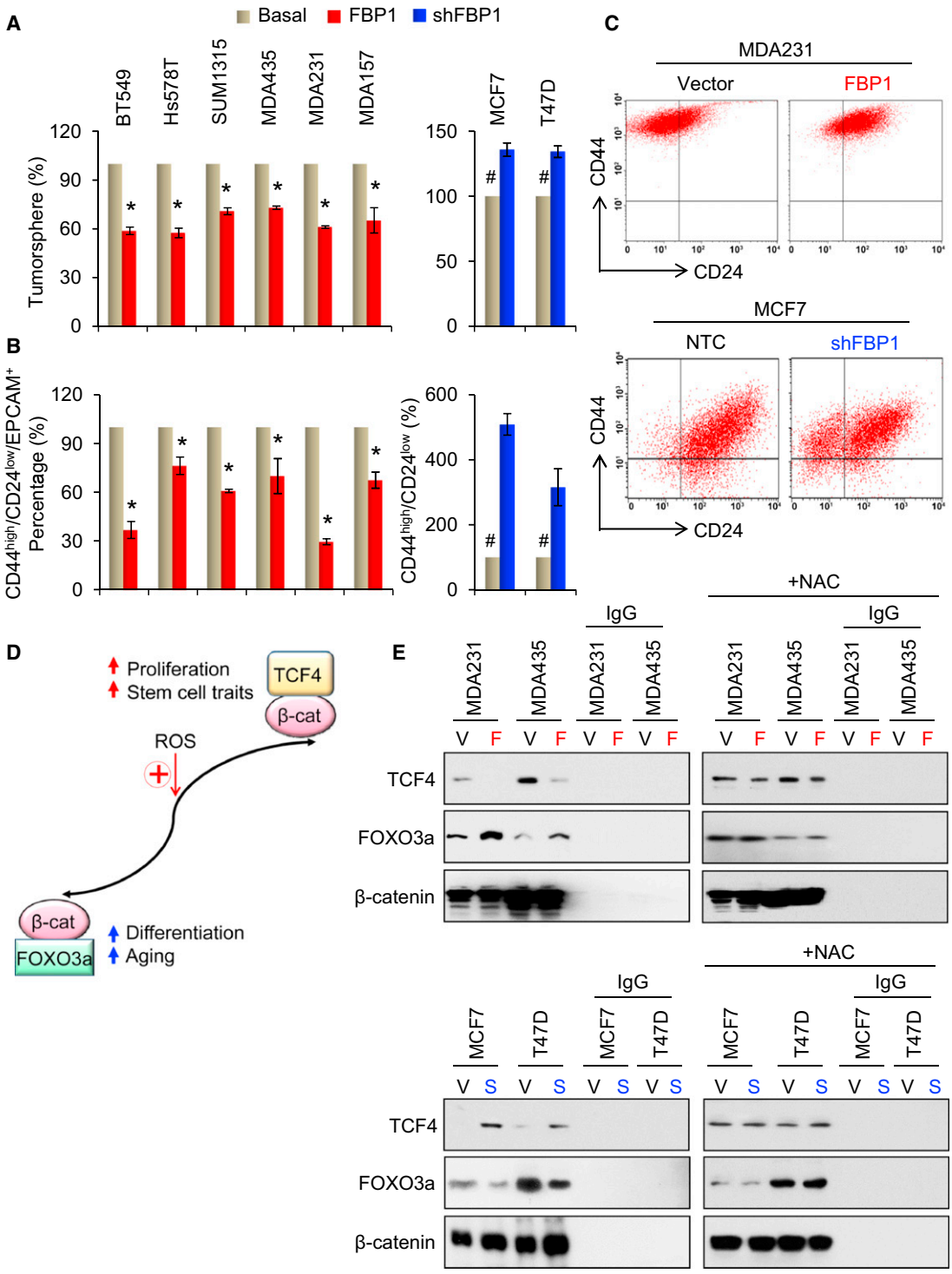

Figure 7. FBP1 Inhibits Tumorsphere Formation and Reduces CSC Population

(A) Tumorsphere formation was assessed under normoxic conditions.

(B and C) The CSC population ($CD44^{high}/CD24^{low}/EpCAM^{+}$) was analyzed by flow cytometry. Representative images for MDA-MB231 and MCF7 cells are shown in (C).

(D) Schematic diagram of the interaction of β-catenin with TCF4 and FOXO3a.

(E) FBP1-expressing BLBC cells (F) as well as in FBP1-knockdown luminal cells (S) were treated with or without NAC overnight; the interactions of β-catenin with TCF4 and FOXO3a were examined by immunoprecipitating β-catenin following immunoblot of TCF4 and FOXO3a.

For A and B, data are presented as a percentage of vector control values (mean ± SD in three separate experiments in duplicates). *$p < 0.01$ and #$p < 0.01$ for vector control cells compared with their FBP1-expressing or FBP1-knockdown clones, respectively.

See also Figure S7.

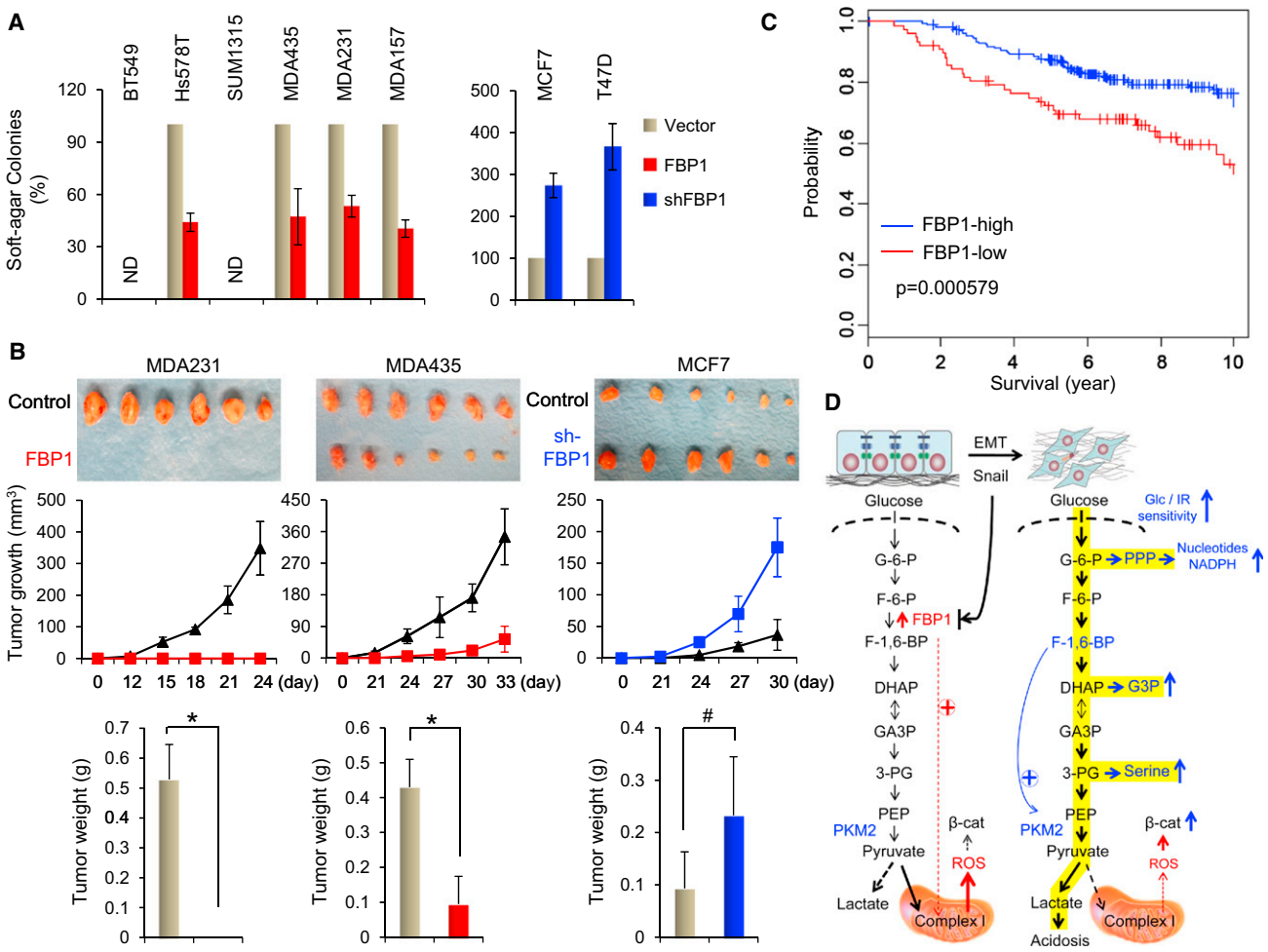

Figure 8. FBP1 Suppresses Tumorigenicity In Vitro and In Vivo

(A) Data of soft-agar assay are presented as a percentage of vector control cell lines (mean ± SD in three separate experiments with duplicates). ND, no colonies detected.

(B) Tumor growth was monitored every 3 days; tumor size and weight were recorded. Data are represented as mean ± SEM from six mice. *$p < 0.01$ and #$p < 0.01$ for vector control cells compared with their FBP1-expressing or FBP1-knockdown clones, respectively.

(C) Kaplan-Meier overall survival curve separates the tumors into two groups based on FBP1 expression.

(D) A proposed model to illustrate the transcription repression of FBP1 by Snail in EMT and BLBC, which results in the switch to aerobic glycolysis and increased β-catenin activity.

See also Figure S8.

analyzer (Seahorse Bioscience, Chicopee, MA). To allow comparison between experiments, data are presented as OCR in pMol/min/104 cells. Basal OCR were measured four times and plotted as a function of cells with and without treatment under the basal condition followed by the sequential addition of oligomycin (1 μg/ml) and FCCP (1 μM) as indicated. The progress curve is annotated to show the relative contribution of basal, ATP-linked and maximal oxygen consumption after the addition of FCCP, and the reserve capacity of the cells. The intracellular concentration of F-1,6-BP was examined by treating cells with 1.25 ml of perchloric acid; cells were then pelleted by centrifugation at 2500× g for 10 min. The cell pellet was resuspended in 0.2 ml of perchloric acid (6%) and 0.2 ml of water. After centrifugation, the pH of the combined supernatant was adjusted to 3.5 with 1% potassium carbonate. F-1,6-BP in the supernatant was determined spectrophotometrically by measuring the decrease of NADH to NAD^+ at 340 nm. Complex I specific activity was assayed as described by Sinthupibulyakit (Sinthupibulyakit et al., 2010) by following the decrease in absorbance due to the oxidation of NADH at 340 nm. The activity was calculated by the differences with and without the complex I inhibitor, rotenone.

For the [U-$^{13}C_6$]-glucose tracer experiment, Vector- and FBP1-expressing MDA-MB231 cells were cultured in the DMEM medium with glucose replaced by 0.1% $^{13}C_6$-glucose for 24 hr. Polar metabolites were extracted from cells and media using the acetonitrile/water/chloroform partitioning and 10% trichloracetic acid methods, respectively. The extracts were subjected to 1D ^1H and $^1H\{^{13}C\}$ HSQC NMR and GC-MS analysis, as previously described (Fan et al., 2011; Le et al., 2012).

DNA Methylation Analysis, ChIP, Quantitative Real-Time PCR, and Luciferase Reporter Assay

The methods used are described in the Supplemental Experimental Procedures.

Metabolic Assays, Colony Formation Assay, Mammosphere Assay, and Flow Cytometry Analysis

All methods are described in detail in the Supplemental Experimental Procedures.

Xenograft Studies

Female ICR-SCID mice (6–8 weeks old) were purchased from Taconic (Germantown, NY) and maintained and treated under specific pathogen-free conditions. All procedures were approved by the Institutional Animal Care and Use Committee at the University of Kentucky College of Medicine and conformed to the legal mandates and federal guidelines for the care and maintenance of laboratory animals. The mice were injected with 1×10^6 FBP1-expressing or knockdown cells on the right MFP and control cells on the left MFP. The mice were then randomly divided into two groups: standard water supply and water supplemented with 40 mM NAC. Tumor formation was examined every 2 to 3 days for the whole duration of the experiment. Tumors were harvested and weighed at the experimental endpoint, and the tumor mass derived from cells with FBP1 expression or knockdown and vector control in both flanks of each mouse were compared.

Statistical Analysis

Experiments were repeated at least twice. Results are expressed as mean ± SD or SEM as indicated. An independent Student's t test was performed to analyze the assay results; a two-tailed Student's t test was used to compare the intergroup differences. A p value < 0.05 was considered statistically significant.

ACCESSION NUMBERS

Microarray data of FBP1 expression in MDA-MB231 and Hs578T cells were deposited at the Gene Expression Omnibus with the accession number GSE41158.

SUPPLEMENTAL INFORMATION

Supplemental Information includes eight figures and Supplemental Experimental Procedures and can be found with this article online at http://dx.doi.org/10.1016/j.ccr.2013.01.022.

ACKNOWLEDGMENTS

We thank Ms. Ramya Balasubramaniam for technical assistance in metabolomics experiments, Dr. Sam Arumugam at J.G. Brown Cancer Center NMR facility for NMR data acquisition, and Dr. Cathy Anthony for critical reading and editing of this manuscript. This work was supported by grants from NIH (CA125454 to B.P.Z.; CA049797 and CA073599 to D.St.C.; P20CA1530343 to B.M.E.; CA118434-01A2 and 1R01ES022191-01 to T.W.M.F.), Susan G Komen Foundation (KG081310), Mary Kay Ash Foundation (to B.P.Z.), National Science Foundation (EPS-0447479 to T.W.M.F.), Edward P. Evans Foundation (to D.St.C.), and pre-doctoral fellowship (BC101068) from DoD Breast Cancer Research Program (to Y.L.).

Received: April 1, 2012
Revised: September 25, 2012
Accepted: January 29, 2013
Published: February 28, 2013

REFERENCES

Blick, T., Hugo, H., Widodo, E., Waltham, M., Pinto, C., Mani, S.A., Weinberg, R.A., Neve, R.M., Lenburg, M.E., and Thompson, E.W. (2010). Epithelial mesenchymal transition traits in human breast cancer cell lines parallel the CD44(hi/)CD24 (lo/-) stem cell phenotype in human breast cancer. J. Mammary Gland Biol. Neoplasia *15*, 235–252.

Bowerman, B. (2005). Cell biology. Oxidative stress and cancer: a beta-catenin convergence. Science *308*, 1119–1120.

Chatterjee, A., Dasgupta, S., and Sidransky, D. (2011). Mitochondrial subversion in cancer. Cancer Prev. Res. (Phila.) *4*, 638–654.

Chen, M., Zhang, J., Li, N., Qian, Z., Zhu, M., Li, Q., Zheng, J., Wang, X., and Shi, G. (2011). Promoter hypermethylation mediated downregulation of FBP1 in human hepatocellular carcinoma and colon cancer. PLoS ONE *6*, e25564.

Christofk, H.R., Vander Heiden, M.G., Harris, M.H., Ramanathan, A., Gerszten, R.E., Wei, R., Fleming, M.D., Schreiber, S.L., and Cantley, L.C. (2008). The M2 splice isoform of pyruvate kinase is important for cancer metabolism and tumour growth. Nature *452*, 230–233.

Crabtree, H.G. (1929). Observations on the carbohydrate metabolism of tumours. Biochem. J. *23*, 536–545.

Dang, C.V., Kim, J.W., Gao, P., and Yustein, J. (2008). The interplay between MYC and HIF in cancer. Nat. Rev. Cancer *8*, 51–56.

Dhasarathy, A., Phadke, D., Mav, D., Shah, R.R., and Wade, P.A. (2011). The transcription factors Snail and Slug activate the transforming growth factor-beta signaling pathway in breast cancer. PLoS ONE *6*, e26514.

Diehn, M., Cho, R.W., Lobo, N.A., Kalisky, T., Dorie, M.J., Kulp, A.N., Qian, D., Lam, J.S., Ailles, L.E., Wong, M., et al. (2009). Association of reactive oxygen species levels and radioresistance in cancer stem cells. Nature *458*, 780–783.

DiMeo, T.A., Anderson, K., Phadke, P., Fan, C., Perou, C.M., Naber, S., and Kuperwasser, C. (2009). A novel lung metastasis signature links Wnt signaling with cancer cell self-renewal and epithelial-mesenchymal transition in basal-like breast cancer. Cancer Res. *69*, 5364–5373.

Dong, C., Wu, Y., Yao, J., Wang, Y., Yu, Y., Rychahou, P.G., Evers, B.M., and Zhou, B.P. (2012). G9a interacts with Snail and is critical for Snail-mediated E-cadherin repression in human breast cancer. J. Clin. Invest. *122*, 1469–1486.

Elstrom, R.L., Bauer, D.E., Buzzai, M., Karnauskas, R., Harris, M.H., Plas, D.R., Zhuang, H., Cinalli, R.M., Alavi, A., Rudin, C.M., and Thompson, C.B. (2004). Akt stimulates aerobic glycolysis in cancer cells. Cancer Res. *64*, 3892–3899.

Emery, J.L., Howat, A.J., Variend, S., and Vawter, G.F. (1988). Investigation of inborn errors of metabolism in unexpected infant deaths. Lancet *2*, 29–31.

Essers, M.A., de Vries-Smits, L.M., Barker, N., Polderman, P.E., Burgering, B.M., and Korswagen, H.C. (2005). Functional interaction between beta-catenin and FOXO in oxidative stress signaling. Science *308*, 1181–1184.

Facucho-Oliveira, J.M., and St John, J.C. (2009). The relationship between pluripotency and mitochondrial DNA proliferation during early embryo development and embryonic stem cell differentiation. Stem Cell Rev. *5*, 140–158.

Fan, T.W., Lane, A.N., Higashi, R.M., Farag, M.A., Gao, H., Bousamra, M., and Miller, D.M. (2009). Altered regulation of metabolic pathways in human lung cancer discerned by (13)C stable isotope-resolved metabolomics (SIRM). Mol. Cancer *8*, 41.

Fan, T.W., Yuan, P., Lane, A.N., Higashi, R.M., Wang, Y., Hamidi, A.B., Zhou, R., Guitart, X., Chen, G., Manji, H.K., and Kaddurah-Daouk, R. (2010). Stable isotope-resolved metabolomic analysis of lithium effects on glial-neuronal metabolism and interactions. Metabolomics *6*, 165–179.

Fan, T.W., Lane, A.N., Higashi, R.M., and Yan, J. (2011). Stable isotope resolved metabolomics of lung cancer in a SCID mouse model. Metabolomics *7*, 257–269.

Fan, T.W.M., and Lane, A.N. (2008). Structure-based profiling of metabolites and isotopomers by NMR. Prog. Nucl. Magn. Reson. Spectrosc. *52*, 69–117.

Koeck, T., Olsson, A.H., Nitert, M.D., Sharoyko, V.V., Ladenvall, C., Kotova, O., Reiling, E., Ronn, T., Parikh, H., Taneera, J., et al. (2011). A common variant in TFB1M is associated with reduced insulin secretion and increased future risk of type 2 diabetes. Cell Metab. *13*, 80–91.

Koppenol, W.H., Bounds, P.L., and Dang, C.V. (2011). Otto Warburg's contributions to current concepts of cancer metabolism. Nat. Rev. Cancer *11*, 325–337.

Le, A., Lane, A.N., Hamaker, M., Bose, S., Gouw, A., Barbi, J., Tsukamoto, T., Rojas, C.J., Slusher, B.S., Zhang, H., et al. (2012). Glucose-independent glutamine metabolism via TCA cycling for proliferation and survival in B cells. Cell Metab. *15*, 110–121.

Li, M.V., Chang, B., Imamura, M., Poungvarin, N., and Chan, L. (2006). Glucose-dependent transcriptional regulation by an evolutionarily conserved glucose-sensing module. Diabetes *55*, 1179–1189.

Liu, X., Wang, X., Zhang, J., Lam, E.K., Shin, V.Y., Cheng, A.S., Yu, J., Chan, F.K., Sung, J.J., and Jin, H.C. (2010). Warburg effect revisited: an epigenetic link between glycolysis and gastric carcinogenesis. Oncogene *29*, 442–450.

Lunt, S.Y., and Vander Heiden, M.G. (2011). Aerobic glycolysis: meeting the metabolic requirements of cell proliferation. Annu. Rev. Cell Dev. Biol. *27*, 441–464.

Manolagas, S.C., and Almeida, M. (2007). Gone with the Wnts: beta-catenin, T-cell factor, forkhead box O, and oxidative stress in age-dependent diseases of bone, lipid, and glucose metabolism. Mol. Endocrinol. *21*, 2605–2614.

Mazurek, S., Boschek, C.B., Hugo, F., and Eigenbrodt, E. (2005). Pyruvate kinase type M2 and its role in tumor growth and spreading. Semin. Cancer Biol. *15*, 300–308.

Metodiev, M.D., Lesko, N., Park, C.B., Camara, Y., Shi, Y., Wibom, R., Hultenby, K., Gustafsson, C.M., and Larsson, N.G. (2009). Methylation of 12S rRNA is necessary for in vivo stability of the small subunit of the mammalian mitochondrial ribosome. Cell Metab. *9*, 386–397.

Mohyeldin, A., Garzon-Muvdi, T., and Quinones-Hinojosa, A. (2010). Oxygen in stem cell biology: a critical component of the stem cell niche. Cell Stem Cell *7*, 150–161.

Peterson, C.W., Stoltzman, C.A., Sighinolfi, M.P., Han, K.S., and Ayer, D.E. (2010). Glucose controls nuclear accumulation, promoter binding, and transcriptional activity of the MondoA-Mlx heterodimer. Mol. Cell. Biol. *30*, 2887–2895.

Polyak, K. (2011). Heterogeneity in breast cancer. J. Clin. Invest. *121*, 3786–3788.

Polyak, K., and Weinberg, R.A. (2009). Transitions between epithelial and mesenchymal states: acquisition of malignant and stem cell traits. Nat. Rev. Cancer *9*, 265–273.

Robey, R.B., and Hay, N. (2009). Is Akt the "Warburg kinase"?-Akt-energy metabolism interactions and oncogenesis. Semin. Cancer Biol. *19*, 25–31.

Sinthupibulyakit, C., Ittarat, W., St Clair, W.H., and St Clair, D.K. (2010). p53 Protects lung cancer cells against metabolic stress. Int. J. Oncol. *37*, 1575–1581.

Thiery, J.P., Acloque, H., Huang, R.Y., and Nieto, M.A. (2009). Epithelial-mesenchymal transitions in development and disease. Cell *139*, 871–890.

van de Vijver, M.J., He, Y.D., van't Veer, L.J., Dai, H., Hart, A.A., Voskuil, D.W., Schreiber, G.J., Peterse, J.L., Roberts, C., Marton, M.J., et al. (2002). A gene-expression signature as a predictor of survival in breast cancer. N. Engl. J. Med. *347*, 1999–2009.

van Poelje, P.D., Potter, S.C., Chandramouli, V.C., Landau, B.R., Dang, Q., and Erion, M.D. (2006). Inhibition of fructose 1,6-bisphosphatase reduces excessive endogenous glucose production and attenuates hyperglycemia in Zucker diabetic fatty rats. Diabetes *55*, 1747–1754.

van 't Veer, L.J., Dai, H., van de Vijver, M.J., He, Y.D., Hart, A.A., Mao, M., Peterse, H.L., van der Kooy, K., Marton, M.J., Witteveen, A.T., et al. (2002). Gene expression profiling predicts clinical outcome of breast cancer. Nature *415*, 530–536.

Ward, P.S., and Thompson, C.B. (2012). Metabolic reprogramming: a cancer hallmark even warburg did not anticipate. Cancer Cell *21*, 297–308.

Zeilstra, J., Joosten, S.P., Dokter, M., Verwiel, E., Spaargaren, M., and Pals, S.T. (2008). Deletion of the WNT target and cancer stem cell marker CD44 in Apc(Min/+) mice attenuates intestinal tumorigenesis. Cancer Res. *68*, 3655–3661.